Journal of Ultrafine Grained and Nanostructured Materials
https://jufgnsm.ut.ac.ir
Vol. 59, No.1, June 2026, pp. 104-115
Print ISSN: 2423-6845 Online ISSN: 2423-6837
DOI: 10.22059/jufgnsm.2026.01.08

Minute-Scale Effective Eradication of *Escherichia coli* and *Staphylococcus aureus* by Silver Nanoparticles: Balancing Efficacy with Osteoblastic Viability (MC3T3 E1)

Hossein Ahmadi[1], Radin Moradi[2], Mohammad Reza Barati[3]*, Seyed Farshid Kashani-Bozorg[1]*

[1] School of Metallurgy and Materials Engineering, College of Engineering, University of Tehran, Tehran, Iran.
[2] Department of Mechanical and Materials Engineering, Queen's University, Kingston, ON K7L 3N6, Canada.
[3] Department of Advanced Materials and New Technologies, Iranian Research Organization for Science and Technology (IROST), Tehran, Iran.

Recieved: 19 May 2026; Accepted: 27 June 2026

[*]Corresponding author, E-mail: Mohammad.barati@irost.ir, fkashani@ut.ac.ir

ABSTRACT

In the present study, highly pure silver nanoparticles (AgNPs) were synthesized using a microwave-assisted precipitation method, which yielded pure AgNPs within a 3-minute reaction time. X-ray diffraction (XRD) analysis confirmed that all of the synthesized nanoparticles possessed a pure phase and a face-centered cubic (FCC) crystal structure. Field emission scanning electron microscopy (FESEM) was subsequently employed to verify the pseudo-spherical morphology of the AgNPs, which exhibited an average particle size distribution of approximately 77.4 nm. The prepared nanoparticles were further characterized by high-resolution transmission electron microscopy (HRTEM), and the results corroborated both the SEM and XRD findings. The AgNPs demonstrated enhanced antibacterial activity against *E. coli* and *S. aureus* when compared with gentamicin, achieving a ≥ 4-$\log_{10}$ reduction in colony-forming units (from ~10^5 to < 10 CFU/ml, the assay detection limit) within 30 minutes at 50 µg/ml. Remarkably, these AgNPs exhibited exceptional biocompatibility with MC3T3-E1 preosteoblast cells, retaining 75.5% viability at the antibacterial working concentration (50 µg/ml) after 48 h, with the half-maximal inhibitory concentration (IC_{50}) remaining above the tested range (> 50 µg/ml). This favorable therapeutic window, rapid pathogen eradication at concentrations well below cytotoxic thresholds, positions these AgNPs as promising candidates for wound management and as a supplementary ingredient for root canal disinfection, ensuring optimal pathogen clearance without compromising healthy cells.

Keywords: *AgNPs; Microwave-assisted; Antibacterial; Dynamic contact; CFU.*

1. Introduction

The emergence of nanotechnology has brought about transformative changes across various domains, including medical therapeutics, environmental remediation, and water treatment, largely through the design of multifunctional nanomaterials endowed with distinctive physicochemical characteristics [1–3]. Within this class of materials, metallic nanoparticles, especially those composed of AgNPs, have garnered substantial interest owing to their remarkable antimicrobial, catalytic, and sensing capabilities [4–6]. Their efficacy against a wide array of both Gram-positive and Gram-negative bacteria has positioned AgNPs among the most potent and adaptable antimicrobial agents documented in the scientific literature [7–9]. Notable examples of susceptible Gram-positive bacteria include

Staphylococcus aureus (S. aureus), *Streptococcus mutans*, and *Enterococcus faecalis*, whereas commonly targeted Gram-negative species encompass *Escherichia coli (E. coli)*, *Pseudomonas aeruginosa*, and *Salmonella typhimurium* [10].

The antimicrobial mechanism of AgNPs may be associated with three interrelated pathways that function synergistically. These consist of: the induction of oxidative stress via the production of reactive oxygen species (ROS) [11], the release of Ag^+ ions capable of binding to and disrupting essential biomolecules [12], and direct, nonoxidative damage to bacterial membranes, proteins, and genetic material [13]. The collective outcome of these actions is the impairment of cellular integrity and metabolic processes, culminating in bacterial cell death.

In light of their considerable antimicrobial promise, a variety of fabrication strategies have been established for producing AgNPs. These include chemical reduction techniques [14], green synthesis mediated by plant extracts [15] or microbial organisms [16], and the Tollens process [17], each offering precise control over particle dimensions and colloidal stability. Ongoing research has increasingly focused on a straightforward synthesis route involving microwave-assisted co-precipitation, followed by rigors structural and morphological characterization as well as assessment of antibacterial effectiveness. This methodology enables rapid production, enhanced material purity, and robust antimicrobial activity, thereby representing a highly promising strategy for the engineering of next-generation antimicrobial agents.

2. Materials and Methods

Following the protocol detailed in our earlier study [18], a microwave-assisted approach was employed for the fabrication of AgNPs, enabling rapid and highly efficient synthesis. Initially, two separate solutions were prepared by dissolving 23.62 mg of silver nitrate ($AgNO_3$, 99% purity, Merck, Darmstadt, Germany) and 26.3 mg of sodium borohydride ($NaBH_4$, 96% purity, Merck, Darmstadt, Germany) each in 20 ml of deionized water. The silver nitrate solution was stirred magnetically until fully dissolved, after which the sodium borohydride solution was added dropwise at ambient temperature under continuous agitation. Once the mixture was prepared, it was transferred to a domestic microwave oven (Feller MW350G, Günselsdorf, Austria; 450 W, 2.45 GHz) equipped with an integrated reflux condenser and water-cooling system to avoid overheating or splashing. Under these reflux-controlled conditions, black precipitates appeared at the bottom of the flask within 3 minutes, indicating successful nanoparticle formation. The resulting nanoparticles were then collected by centrifugation using deionized water three times at 4000 RPM for four minutes each cycle, followed by drying at 50°C.

To characterize the synthesized nanoparticles, multiple analytical techniques were employed. X-ray diffraction (XRD, Rigaku Ultima VI, Tokyo, Japan) using Cu-K_α radiation (λ = 1.5405 Å) operated at 40 kV was utilized to examine crystal structure and phase composition across a 2θ range of 5°–80°. Morphological features and particle size distribution were assessed via field emission scanning electron microscopy (FESEM, Hitachi S-4160), while elemental composition was determined using energy-dispersive X-ray spectroscopy (EDS). Further investigation of nanoscale morphology and crystallographic details was conducted with high-resolution transmission electron microscopy (HRTEM, FEI Tecnai G2 F20 SuperTwin, Oregon, USA) operating at an accelerating voltage of 200 kV.

The bactericidal activity of the synthesized AgNPs was assessed compared to gentamicin to treat *Staphylococcus aureus* (ATCC 25923) as the Gram-positive strain and *Escherichia coli* (ATCC 25922) as the Gram-negative strain, both obtained from Bahar Afshan, Tehran, Iran. The evaluation followed the "Standard Test Method for Determining the Antimicrobial Activity of Immobilized Antimicrobial Agents Under Dynamic Contact Conditions" (ASTM E2149–10), subsequently using the spread plate method to determine bacterial resistance. The data represent a single time-point endpoint, not a kinetic series.

A bacterial inoculum of 1 ml was first prepared in Muller–Hinton broth and adjusted to a 0.5 McFarland standard (approximately 1.5×10^8 CFU/ml). This inoculum was then serially diluted with sterile physiological saline at pH 7.0 to obtain a working bacterial suspension with a final concentration of 1×10^5 CFU/ml. Following this, the final concentration of AgNPs was adjusted to 50 µg/ml to treat the bacteria. Identical experimental conditions were applied to both negative and positive controls. For the positive control, a gentamicin solution diluted from an initial concentration of 40 mg/ml to a final concentration of 100 µg/ml was used. In contrast, the negative control consisted of a nanoparticle-free blank solution, which allowed for the assessment of normal bacterial proliferation in the absence of any inhibitory substance. All flasks were securely capped and placed in a wrist-action incubator shaker set to 120 rpm at a constant temperature of 37°C. Following a 30-minute exposure period, samples were extracted and subjected to tenfold serial dilution using physiological saline. From each dilution, 100

μL was transferred onto tryptic soy agar plates (supplied by Zistkaavesh Iranian Co., Tehran, Iran) to enumerate viable colonies. The plates were then incubated at 30 ± 2°C for 48 h. After this incubation period, colony counts were recorded, and the remaining bacterial population was calculated and reported as colony-forming units per milliliter (CFU/ml). The limit of detection (*LOD*) for this assay was calculated as follows: plating volume = 100 μl (0.1 ml); dilution factor for neat sample = 1; therefore, *LOD* = 1 / (0.1 ml × 1) = 10 CFU/ml. Plates exhibiting no visible colonies are reported as < 10 CFU/ml rather than zero.

The MC3T3-E1 preosteoblast cells were obtained from the National Cell Bank at the Pasteur Institute of Iran (Tehran, Iran; NCBI no. C657). For standard growth, the cells were maintained in Dulbecco's Modified Eagle's Medium (DMEM; NY, USA) containing 10% fetal bovine serum (FBS), 100 U/ml penicillin, and 100 μg/ml streptomycin. The culture flasks were kept in a standard humidified incubator at 37°C with 5% CO_2. We replaced the growth medium every three days until the cells reached full confluence. Cells grown purely in this standard medium, without any treatments, acted as our negative control. Once confluent, the cells were harvested using a 0.25% trypsin and 0.05% EDTA solution, and then cells were seeded in the 96-well cell culture plates with a density of 1×10^4 cells per well. Each well contained 100 μL of DMEM with 10% FBS (GIBCO, Scotland). The plates were left for 24 h to allow the cells to adhere to the bottom of the wells. After the cell attachment, the culture medium was replaced with 90 μL of silver nanoparticle (AgNP) suspensions, prepared at concentrations of 1, 5, 10, 20, and 50 μg/ml, mixed with 10 μL of FBS. The cells were exposed to these nanoparticles for either 48 or 72 h under standard incubator conditions, and the treatment fluids were freshly replaced every 24 h.

The cell survival at both time points was evaluated using a standard MTT colorimetric assay, following the ISO 10993-5 standard method. At the end of each exposure period, the suspension containing AgNPs was discarded, and 100 μL of MTT reagent (0.5 mg/ml) was added to every well. The plates were then kept in the dark at 37°C for 4 h. Next, we carefully removed the MTT liquid and added 150 μL of isopropanol (Sigma, USA) to dissolve the dark purple formazan crystals produced by living cells. Finally, we recorded the absorbance at 545 nm using an ELISA microplate reader (Bio Tek ELx808, USA). To find the final cell viability percentage, we normalized the absorbance values of the treated groups against those of the untreated control group. The IC_{50} (the half-maximal inhibitory concentration where viability is reduced to 50%) was calculated using a 3-parameter Hill equation. The 3-parameter Hill equation for viability can be expressed as:

$$y = \frac{\text{Maximum viability}}{1 + (\frac{x}{IC_{50}})^n} \quad (1)$$

Where *y*, *x*, and *n* are viability (%), concentration (μg/ml), and hill coefficient (slope of the curve).

Results obtained from the MTT assay and antibacterial assay were expressed as the mean ± standard deviation, calculated from four independent replicates (n = 4). Differences among the experimental groups were evaluated using a one-way analysis of variance (ANOVA). Statistical significance was established at a threshold of $p < 0.05$.

3. Results and Discussion

XRD was employed to examine the structural characteristics and phase composition of the as-synthesized AgNPs. As shown in Fig. 1, the diffraction pattern revealed four peaks corresponding to the (111), (200), (220), and (311) crystal planes of an FCC structure, consistent with the standard reference pattern for silver (JCPDS card No. 04-0783). Moreover, the lack of any extraneous diffraction peaks confirms the high phase purity of the synthesized nanoparticles. The average crystallite size (D) of these nanoparticles was determined using the Scherrer equation [19]:

$$D = K.\lambda / \beta.\cos(\theta) \quad (2)$$

In this equation, K denotes the shape factor (typically assigned a value of 0.89 for face-centered cubic metals like silver), λ corresponds to the X-ray wavelength, β is the full width at half maximum of the diffraction peak, and θ signifies the Bragg diffraction angle. This calculation yields an estimate of the coherent crystalline domain dimensions within the AgNPs. Applying equation (2), the mean crystallite size of the AgNPs was found to be approximately 21 ± 1 nm.

Figs 2a and 2b display FESEM images of the AgNPs at two different magnifications. Based on these micrographs, the silver nanoparticles exhibit a uniform grain size and a morphology that is approximately spherical. Referring to Fig. 2b, the particle size distribution histogram for the synthesized AgNPs was constructed using *ImageJ* software. As can be observed, the particle size distribution follows a Gaussian trend, ranging from approximately 50 nm to 110 nm, with an average particle size calculated to be 77.4 ± 12 nm. Fig. 2e shows the elemental map corresponding to the entire area imaged in the backscattered-mode FESEM micrograph of Fig. 2d, which further confirms the presence of silver without any trace.

TEM was utilized for additional morphological and crystallographic characterization of the synthesized AgNPs. The TEM micrograph presented in Fig. 3a reveals spherical, electron-dense particles with an average diameter of roughly 77 nm. This value aligns closely with the mean particle size determined from the FESEM images shown in Fig. 2. Notably, this physical particle size (~ 77.4 nm) is substantially larger than the average crystallite size of ~ 21 nm calculated from XRD data, indicating that each AgNP is polycrystalline, where multiple smaller crystallites aggregate and fuse to form a single, larger nanoparticle. This interpretation is directly confirmed by the selected area electron diffraction (SAED) pattern in Fig. 3b, which displays well-defined concentric rings attributable to the (111), (200), (220), (311), and (222) crystallographic planes. These findings correspond remarkably well with the XRD reflection peaks presented in Fig. 1, providing consistent evidence for the face-centered cubic structure of the synthesized AgNPs.

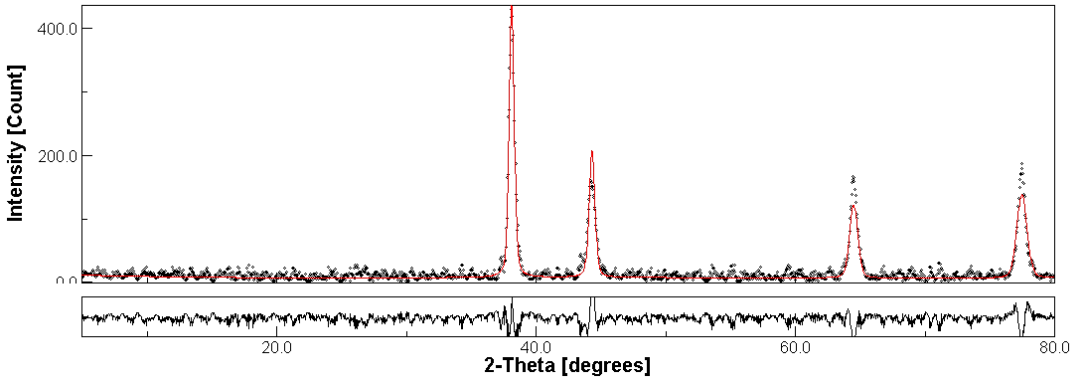

Fig. 1- X-ray diffractogram of AgNPs synthesized by the microwave-assisted method.

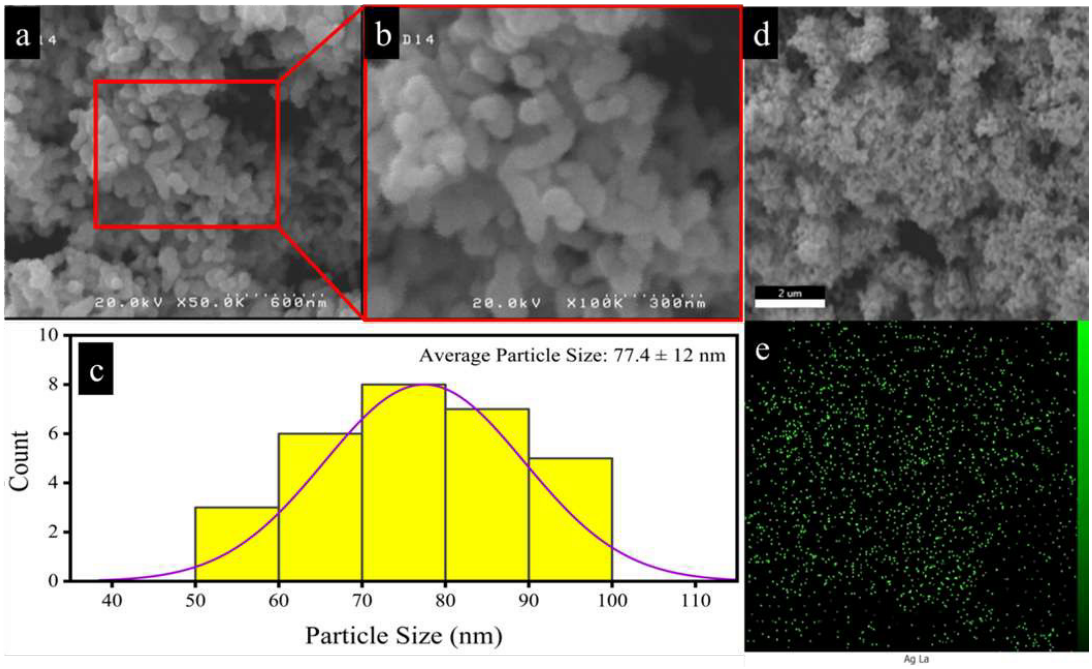

Fig. 2- FESEM images of the AgNPs: secondary electron micrographs captured at magnifications of (a) 50 kX and (b) 100 kX. (c) Histogram representing the particle size distribution. (d) Micrograph acquired using backscattered electron mode, accompanied by (e) the corresponding full-area elemental map for the entire region shown in panel (d).

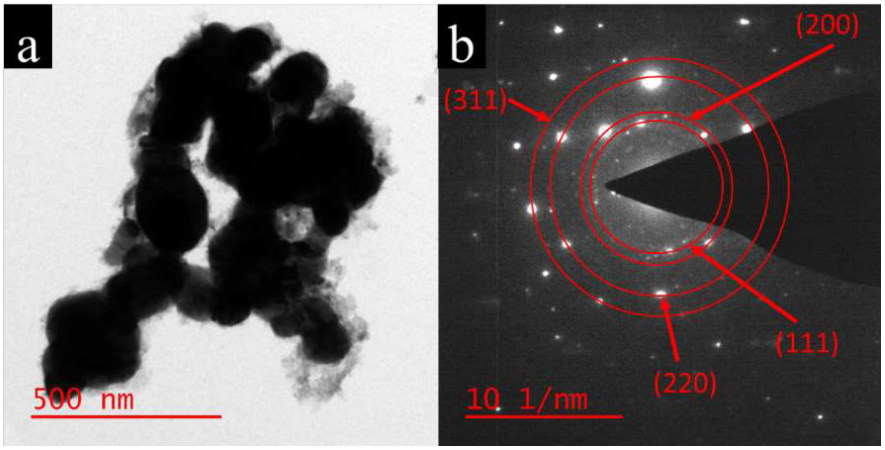

Fig. 3- (a) TEM micrograph and (b) SAED pattern of AgNPs.

Given the substantial body of recent literature documenting the antimicrobial properties of silver nanoparticles, it is necessary to assess the antibacterial potential of the nanoparticles synthesized in the present work. Accordingly, following the structural, chemical, and morphological analyses, antibacterial assays were performed to determine their effectiveness against typical Gram-positive and Gram-negative bacterial strains.

To evaluate this efficacy, two bacterial species were chosen: *E. coli* as a model Gram-negative organism and *S. aureus* as a representative Gram-positive strain. When compared with the reference antibiotic gentamicin, the synthesized Ag NPs demonstrated outstanding antibacterial activity against both bacteria. More specifically, after exposure to AgNPs, the CFU/ml fell from ~ 5×10^4 to < 10 for *S. aureus* and from ~ 8×10^3 to < 10 for *E. coli*. While, under identical test conditions, gentamicin, which is recognized as one of the most frequently prescribed broad-spectrum antibiotics in clinical practice, reduced CFU/ml to < 10 for *S. aureus* and to 28 for *E. coli*. As noted in the methods section, the concentrations of AgNPs and gentamicin were kept equal to ensure a fair comparison of their antimicrobial effectiveness.

The reduction percentage of CFU was calculated using the following equation to quantify the antimicrobial activity:

$$\text{Reduction } (\%) = (B - A)/B \times 100 \quad (3)$$

In this equation, A represents the CFU count of the bacterial suspension exposed to the antibacterial agent after the specified contact period, while B corresponds to the CFU count of the negative control sample maintained under identical conditions.

Within a 30-minute exposure period, the synthesized AgNPs achieved a ≥ 4-$\log_{10}$ reduction in viable bacterial colonies for both *S. aureus* and *E. coli* (from initial inocula of ~10^5 CFU/ml to < 10 CFU/ml, the assay detection limit), demonstrating exceptional antimicrobial performance. Under the same experimental conditions, gentamicin yielded reduction percentages of 99.999% against *S. aureus* and 96% against *E. coli* (as illustrated in Fig. 4). No statistically significant differences were observed between AgNPs and gentamicin for either bacterial strain. It should be noted that error bars are not shown for the Ag NP and gentamicin-exposed *S. aureus* groups in Fig. 4, because both treatments resulted in no visible colonies on any replicate plate. Thereby, the standard error could not be reported due to zero variance. This comparable level of efficacy between AgNPs and gentamicin underscores the considerable promise of AgNPs as effective antimicrobial agents. It is important to note that the reported "complete eradication" refers to a reduction below the assay detection limit (<10 CFU/ml) rather than absolute biological sterility. The initial bacterial load of ~10^5 CFU/ml was reduced by ≥ 4 $\log_{10}$ within 30 minutes, a reduction magnitude that meets and exceeds the criteria for potent bactericidal activity defined by quantitative microbiological standards. This magnitude of reduction represents effective bacterial elimination for practical and clinical applications, while recognizing the inherent detection limits of standard CFU-based plating methods. It should be noted that the present study employed a single exposure time point (30 minutes) according to the ASTM E2149–10 standard; therefore, while our data demonstrate complete bacterial elimination within this timeframe, they do not establish the full time-kill profile or the minimum time required for eradication.

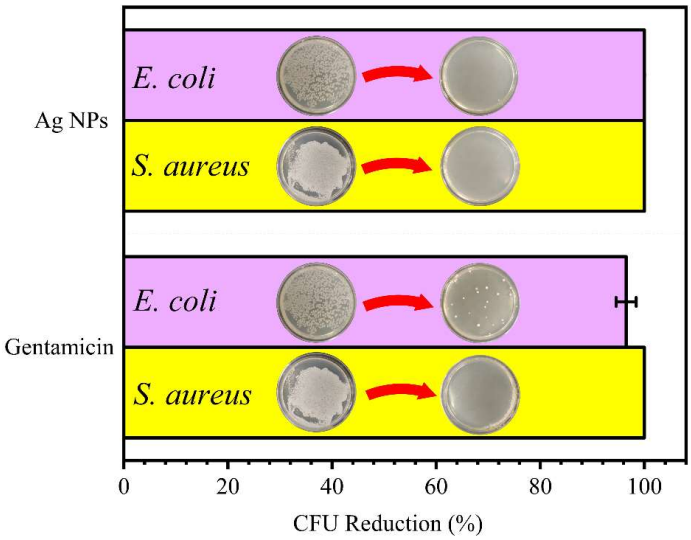

Fig. 4- Comparative CFU reduction (%) of *E. coli* and *S. aureus* exposed to gentamicin versus AgNPs (50 µg/ml, 30 minutes). For AgNP- and gentamicin-treated *S. aureus*, all replicates (n = 4) yielded < 10 CFU/ml (*LOD*). No significant differences were found between AgNPs and gentamicin for either bacterial strain (p > 0.05).

Previous findings on the antibacterial efficacy of silver nanoparticles are briefly summarized in Table 1. The table outlines the synthesis methodology, preparation time, particle dimensions, and morphological characteristics of the produced AgNPs, as well as their antimicrobial activity and test details, all of which are among the most essential properties of AgNPs, based on the literature reviewed from 2015 to 2026.

Compared with the synthesis methods reported in Table 1, the microwaveassisted method used in this study offers several distinct advantages. The most prominent benefit is the extremely short reaction time; AgNPs were produced in approximately 180 seconds. In contrast, many green or conventional methods require reaction times ranging from several minutes to many hours, and occasionally days [22, 24, 26, 31]. This rapid formation is due to the efficient and uniform heating provided by microwave irradiation, which accelerates nucleation and growth.

Another significant advantage is the simplicity of the method. It employs readily available chemicals and a standard microwave system, making the process lowcost and easier to perform than more complex techniques such as laser ablation or biological synthesis. The resulting nanoparticles are predominantly spherical, with a fairly uniform size and high crystallinity, indicating that microwaveassisted synthesis provides excellent control over particle formation.

Regardless of the synthesis method, the antibacterial activity of AgNPs has most commonly been evaluated using the agar diffusion (disk/well) method (Table 1). Although this method is simple and straightforward, it is primarily suitable for initial screening. The high potency of AgNPs as antibacterial agents is well established [20], but agar diffusion cannot provide information on the kinetics or mechanism of bacterial killing. Moreover, the zone of inhibition typically requires 16–24 h to become visible, meaning that the killing process itself is not directly observed within a defined short time frame. Consequently, this method fails to clearly demonstrate how parameters such as particle size, shape, and concentration influence the mechanism or kinetics of bacterial killing. To understand how and how quickly AgNPs kill bacteria, a quantitative and more informative approach, the dynamic contact (timekill) assay, was employed in this study. This method provides a direct measure of bactericidal kinetics using timedependent kill curves [33, 34]. Typically, this assessment reveals killing times on the order of minutes to 1–2 h (e.g., > 99% kill within 60–120 minutes). Our synthesized AgNPs exhibited strong antibacterial activity, eliminating both *E.coli* and *S. aureus* within 30 minutes (Table 1). This performance is comparable to the many previously reported studies, which often require longer incubation times to achieve similar bactericidal endpoints. However, direct comparison with qualitative diffusion-based studies in Table 1 is not methodologically valid. We present Table 1 primarily to illustrate that (i) most AgNP antibacterial studies employ qualitative methods unsuitable for kinetic assessment, and (ii) quantitative dynamic contact studies are infrequently documented, highlighting the value of our approach.

Table 1- Summary of literature-reported synthesized AgNPs

Synthesis Method & Duration	AgNPs Characteristics	Antibacterial Test Details			Ref.
		AgNPs Concentration	Test Method	Other Information	
Green Synthesis, 1 h	~14 nm, spherical	C_{AgNPs} = 1 mM	Agar well diffusion assay (QI*)	24 h incubation at 37 °C. Zones of inhibition (mm): *E. coli* 12.0 ± 0.41; *K. pneumoniae* 11.5 ± 0.62; *P. aeruginosa* 11.4 ± 0.82; *S. aureus* 11.1 ± 0.47; *S. paratyphi* 10.5 ± 0.42. Sterilized distilled water as a negative control	[20]
Microwave-assisted Synthesis, 4 minutes	~59.5 nm, spherical	C_{AgNPs} = 2.5–10 µg/mL	Agar well diffusion assay (QI)	24 h incubation at 37 °C; inhibition zones (mm): *S. aureus* = 16, *E. faecalis* = 10, *E. coli* = 15, *P. aeruginosa* = 19, *S. mutans* = 18, *C. albicans* = 21 at 10 µg/mL. Biofilm inhibition in *P. aeruginosa*: 50% at 10 µg/mL, 80% at 20 µg/mL. Standard antibiotic discs were used as positive controls.	[21]
Green Synthesis, 30 minutes + 24 h	~27 nm, spherical	C_{AgNPs} = 0, 5, 10, 20, 40, 80 µg/mL, agar well diffusion, and broth culture methods	Agar well diffusion and broth culture methods (QI)	Incubation at 37 °C. Zones of inhibition: *E. coli* = 22 mm; *C. albicans* = 20 mm (at 80 µg/mL). Growth kinetic and potency assays confirmed complete inhibition at 40 µg/mL after 4–48 h. Amoxicillin (for *E. coli*) was used as a positive control; the root extract alone served as the negative control.	[22]
Green Synthesis, 15 minutes	~16 nm, spherical	C_{AgNPs} = 1 mM	Kirby–Bauer disc diffusion method (QI)	24 h incubation (bacteria) and 72 h (fungi) at 37 °C. Zone of inhibition (mm): *E. coli* 3–4; *Pseudomonas* 5–8; *Bacillus* 5–6; *Staphylococcus* 3–5; *A. niger* 3–5; *A. flavus* 4–6; *Penicillium* 3–7 (dose-dependent from 2–8 µl).	[23]
Green Synthesis, 48 h	~13.6 nm, spherical	C_{AgNPs} = 1 mM	Modified disc diffusion method (Mueller–Hinton agar)—(QI)	Inoculum = 0.5 McFarland (≈10^8 CFU/ml); incubation = 24 h at 37 °C. Zone of inhibition (mm): *S. aureus* = 15; *S. epidermidis* = 12; *E. coli* = 12; *P. vulgaris* = 11. Streptomycin (1 mg/ml) positive control: *S. aureus* = 17 mm, *E. coli* = 17 mm, *P. vulgaris* = 19 mm, *S. epidermidis* = 0 mm (no inhibition); $AgNO_3$ (1 mM) negative control = no inhibition.	[24]
Chemical, 20 minutes	~52 nm, predominantly spherical	C_{AgNPs} = 0.25–2.0 µg/mL.	Agar plate exposure method (QI)	Bacterial lawns grown at 37 °C; zones of inhibition observed after 24 h. *S. aureus* showed larger zones than *P. aeruginosa* and *E. coli*. Broth microdilution MIC was performed for *S. aureus* (0.25–2.0 µg/ml range tested). Negative control water and trisodium citrate (no inhibition).	[25]
Biological (mycosynthesis), 72 h	10-30 nm, spherical	C_{AgNPs} = 1 mM	Disc diffusion method (QI)	Incubation at 37 °C for 24 h. Zone of inhibition (mm, mean ± SD): *E. coli* 16.50 ± 1.50; *P. aeruginosa* 16.25 ± 1.25; *S. aureus* 15.50 ± 2.50; *B. subtilis* 11.50 ± 2.00. A combination of AgNPs + streptomycin slightly enhanced activity (*E. coli* 18.50 ± 1.00; *P. aeruginosa* 18.25 ± 0.75; *S. aureus* 17.25 ± 2.25; *B. subtilis* 17.75 ± 2.75). Streptomycin (control) zones (mm): *E. coli* — (no inhibition); *P. aeruginosa* 3.00 ± 3.00; *S. aureus* 3.00 ± 3.00; *B. subtilis* 9.25 ± 1.75.	[26]
Photosynthesis, 20 minutes	16.70–33.74 nm, Spherical	C_{AgNPs} = 5, 8, 10, 12, 15 mg/mL	Broth culture assay (QI)	Inoculum = 10^6 CFU/ml (0.5 McFarland); incubation = 24 h at 37 °C. Result: 100% inhibition of all tested strains at all concentrations (5–15 mg/ml).	[27]
Laser ablation in deionized water using Nd:YVO_4 lasers, 1 h	Original (as-ablated) NPs ~35–70 nm; after 3 re-irradiations (G3), mean size reduced to ~10–15 nm (smallest), spherical	C_{AgNPs} = 300 mg/L	Adhesion test (90 minutes) – (QI)	% surface covered measured by fluorescence microscopy–biofilm test (48 h): Confocal laser scanning microscopy (CLSM) used to quantify coverage and thickness. - Best result: Ti discs with AgNPs re-irradiated 3× (G3) showed maximum inhibition of both *S. aureus* and multispecies oral biofilms. - Reduction of surface coverage ≥80–90% and biofilm thickness minimized compared to control. Bare titanium discs (no AgNPs) used as control.	[28]

Table 1- Cont.

Synthesis Method & Duration	AgNPs Characteristics	Antibacterial Test Details			Ref.
		AgNPs Concentration	Test Method	Other Information	
Chemical reduction, 1 h	10–20 nm, spherical	CAgNPs = 0.002 M	Agar well diffusion method (Ql)	Incubation for 24 h at 37 °C. Best results: - For S. aureus: 2.5 mm inhibition zone at $NaBH_4/AgNO_3$ molar ratios of 0.5–2. - For E. coli: 4 mm inhibition zone at the same ratios. High $NaBH_4$ ratios (≥5) caused aggregation, resulting in loss of antibacterial activity.	[29]
Green synthesis, 3 h	~10 nm, spherical	CAgNPs = 1 mM	Agar well diffusion method, 5 mm wells (Ql)	Incubation at 37 °C for 24 h. Best activity: Proteus mirabilis — 14 mm zone of inhibition at 15 µl AgNPs. *Staphylococcus aureus* — 12 mm at 15 µl. Control (no AgNPs): 0 mm inhibition.	[30]
Green synthesis, ~12–24 h	13 nm	CAgNPs = 17 µg/mL.	Agar well diffusion (Ql)	24 h incubation at 37 °C. Best results: • M. luteus: 7.7 ± 0.4 mm (AgNP-S) • E. coli: 6.5 ± 0.3 mm (AgNP-F). Penicillin G (for *M. luteus*) and chloramphenicol (for *E. coli*) were used as positive controls; plant extract, AgNO3, and distilled water were used as negative controls.	[31]
Biogenic green synthesis, 30 minutes	28–41 nm, spherical	CAgNPs = 10, 20, 40, 80, and 160 µg/mL.	Agar well diffusion (Ql)	Incubation for 24 h at 37 °C. Best activity: 14.00 ± 0.58 mm zone of inhibition at 160 µg/ml. MIC: 40.00 ± 5.77 µg/ml (complete inhibition). Growth curve studies showed halted bacterial growth above MIC. Streptomycin (0.1%) as a positive control and DMSO as a negative control.	[32]
Polyol method (Ethylene glycol as reductant and PVP as the capping agent)	30–50 nm, irregular shapes, including some spheres, short rods, and tetrahedrons	CAgNPs = 10–80 µg/mL	Dynamic contact (time-kill) assay (Qn*)	The killing times range from minutes to 3 h (e.g., more than 99% of the targets are killed within 180 minutes).	[33]
Green synthesis using tea leaf extracts	4.06 nm	CAgNPs = 500 µg/mL	Dynamic contact (time-kill) assay (Qn)	>99.9% reduction in CFU/ml within 1–2 h using time-kill curves against *E. coli*.	[34]
Microwaved-assisted method	77.4 ± 12 nm	CAgNPs = 50 µg/mL	Dynamic contact (time-kill) assay (Qn)	>99.9% reduction in CFU/mL within 30 minutes against *E. coli*, and *S. aureus*.	Present study

*Note: The *Ql* and *Qn* represent qualitative and quantitative assessments, respectively.

The primary parameter governing bactericidal activity in the dynamic contact method is particle size. The strong size dependency of AgNP activity can be explained by the "dualfront attack" mechanism, involving both silver ion release and direct contact. Silver ions (Ag^+) are a primary toxic agent; they disrupt the cell membrane, bind to DNA and other vital cellular components, halt replication, and induce reactive oxygen species (ROS) that damage lipids, proteins, and DNA. Concurrently, the physical interaction between the nanoparticle and the bacterial cell is a critical synergistic factor. This contact creates a highly concentrated "hotspot" of ions at the particlecell interface that is far more effective than ions alone in solution, enhances the cellular uptake of particleassociated ions, maximizes internal damage, and can itself rupture the cell membrane and cell wall.

Because the dynamic contact method provides a quantitative measure of these processes, it can be used to determine the kinetics of bacterial killing using a simple differential equation ($n(t) \sim e^{-at}$), thereby quantifying the killing rate of the antimicrobial agent. As a result, this method provides a more accurate measure of the true antibacterial potency of AgNPs. For example, Haque et al. developed an experimentbased quantitative model using

CFU timekill curves, showing that bacteria are killed exponentially in the presence of AgNPs (average sizes of 30 nm and 50 nm, with irregular shapes including some spheres, short rods, and tetrahedrons). They reported complete killing of the initial bacterial inoculum (10^5 CFU/mL) after approximately 3 h, highlighting the significantly comparable bactericidal action achieved in the present study. The remarkably faster kill time (30 minutes versus ~3 h) of AgNPs with a size of 77.4 nm (C_{AgNPs} = 50 µg/mL) in the present study, with respect to the AgNPs with sizes of 30-50 nm and C_{AgNPs} = 10-80 µg/mL reported in [33], is a direct result of several factors such as particle morphology, surface chemistry, and capping agents.

The microwave-assisted synthesis may have preferentially produced a shape, such as spherical NPs with high uniformity (Fig. 2 and Fig. 3), known for their potent activity, providing a more favorable interaction with bacterial surfaces. In contrast, the particles in Haque et al. [33] exhibited a mixed, irregular morphology, which could reduce their overall efficacy. Furthermore, the capping PVP molecules on their AgNPs could reduce the release of Ag^+ at the bacteria–AgNPs interface, reducing the antibacterial activity.

In another study, Liao, S., et al. [34] found the AgNPs were fast-acting, achieving a > 99.9% reduction in CFU/mL within 1–2 h using time-kill curves against *E. coli*. It is interesting to mention that even with the use of highly concentrated AgNPs with C_{AgNPs} = 500 µg/mL, were not able to eliminate *E. coli* (10^6 CFU/mL) in less than 30 minutes, confirming enhanced antimicrobial activity of AgNPs synthesized in this study. Despite the small particle size enabling AgNPs to adhere to the cell wall and penetrate into the bacteria cell easily, which in turn improves their antimicrobial activity, the green synthesis of AgNPs by using tea leaf extracts causes a coating capping agent (amine-I group) on the surface of AgNPs, which increases the hydrodynamic size of nanoparticles and potentially limits Ag^+ release [34], which in turn reduces the antimicrobial activity compared with the AgNPs in the present study.

The enhanced antimicrobial performance of these AgNPs may be favorably influenced by the microwave-assisted synthesis, which yields highly uniform, spherical, and crystalline nanoparticles. By avoiding the use of inhibitory capping agents found in other studies, which often hinder contact and prolong kill times, it is expected that this method may maximize Ag^+ release and direct bacteria-particle interactions, establishing a potent and rapid-acting antimicrobial platform. Remarkably, despite this aggressive action against pathogens within a couple of minutes (less than 1 h), the nanoparticles demonstrate impressive biocompatibility with osteoblastic cells in the short term. As shown in Fig. 5 and Table 2, while exposure at 48 h does cause a statistically significant reduction in viability compared to the control ($p < 0.05$), the cells are largely unaffected at low-to-mid doses (1 to 20 µg/mL), maintaining a remarkably high survival rate of 97.0% to 92.2%. A substantial cytotoxic effect only emerges at the maximum dose of 50 µg/mL, where viability drops to 75.5%. Ultimately, because the IC_{50} remains well above 50 µg/mL at 48 h, these findings confirm that the nanoparticles successfully balance potent antimicrobial efficacy with a high degree of early-stage biocompatibility.

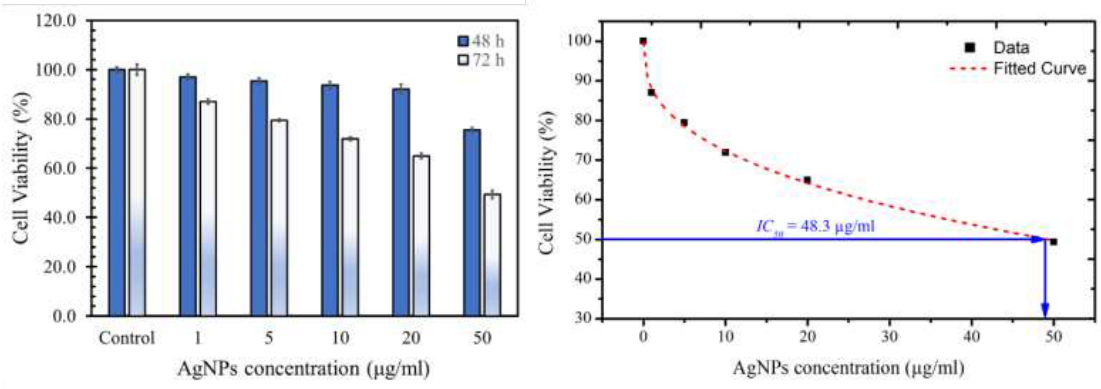

Fig. 5- (a) Viability percentages of MC3T3-E1 cells after treatment with different concentrations of AgNPs for 48 h and 72h, and (b) Sigmoidal curve for MTT assay of cell with AgNPs after 72 h, showing IC_{50} value.

Table 2- Pairwise p-values from one-way ANOVA comparing AgNP-treated groups to the control sample at 48 h, 72 h, and between time points, with four replicates (n = 4) per group

Comparison	Time point	p-value	Significant
Control vs. 1 (μg/ml)	48 h	0.0099	** ($p < 0.01$)
	72 h	4.2×10^{-5}	**** ($p < 0.0001$)
Control vs. 5 (μg/ml)	48 h	0.0013	** ($p < 0.01$)
	72 h	1.7×10^{-6}	**** ($p < 0.0001$)
Control vs. 10 (μg/ml)	48 h	0.00039	*** ($p < 0.001$)
	72 h	2.6×10^{-7}	**** ($p < 0.0001$)
Control vs. 20 (μg/ml)	48 h	0.00048	*** ($p < 0.001$)
	72 h	7.6×10^{-8}	**** ($p < 0.0001$)
Control vs. 50 (μg/ml)	48 h	4.1×10^{-10}	**** ($p < 0.0001$)
	72 h	1.3×10^{-10}	**** ($p < 0.0001$)
1 (μg/ml)	Between 48 & 72	1.4×10^{-5}	**** ($p < 0.0001$)
5 (μg/ml)		1.2×10^{-7}	**** ($p < 0.0001$)
10 (μg/ml)		2.3×10^{-8}	**** ($p < 0.0001$)
20 (μg/ml)		1.2×10^{-7}	**** ($p < 0.0001$)
50 (μg/ml)		2.0×10^{-9}	**** ($p < 0.0001$)

Note: Significance levels are indicated as follows: **$p < 0.01$, ***$p < 0.001$, and ****$p < 0.0001$ (all comparisons are significant at *$p < 0.05$).

At 72 h, the effect is even stronger; all pairwise differences are highly significant ($p \ll 0.001$). In fact, for every non-zero concentration, viability is lower at 72 h than at 48 h, indicating that longer exposure intensifies the cytotoxicity. At prolonged exposure of 72 h, the fitted curve on the viability percentage against AgNPs concentration is sigmoidal (Fig. 5b). The calculated IC_{50} according to Fig. 5b and Hill slope (n) ≈ 0.6 is around ~ 48.3 μg/ml, meaning that prolonged incubation effectively lowers the half-maximal inhibitory concentration to within the tested range. Therefore, the AgNPs at 72 h exposure to the MC3T3-E1 cells display potent, dose-dependent anti-proliferative activity, with a clear therapeutic window established. This suggests a cumulative mechanism: the longer the cells are exposed, the more Ag^+ ions are internalized and released, leading to progressive mitochondrial dysfunction and cell death (MC3T3-E1 cells). Further, between 48 h and 72 h, the drop in viability over time is significantly greater for each treated group than for the control ($p < 0.0001$ for all pairs). This confirms that the AgNPs cause a timedependent cytotoxic effect beyond the baseline change seen in untreated cells.

The synthesized AgNPs demonstrate an exceptional balance between potent antimicrobial efficacy and mammalian cell biocompatibility. At the antibacterial working concentration of 50 μg/ml, MC3T3-E1 preosteoblasts retained 75.5% viability at 48 h, with the IC_{50} remaining above the tested concentration range (>50 μg/ml). While cell line differences preclude direct comparison, this profile appears favorable relative to literature reports: Dinc et al. [35] reported an IC_{50} of 38 μg/ml for human vein endothelial cells (HUVECs) with 55 nm AgNPs, while Paknejadi et al. [36] observed IC_{50} values of 30.64 and 14.98 μg/ml for human skin fibroblasts at 24 h and 48 h, respectively, using smaller (6 nm) PVP-coated particles. The apparent difference may reflect cell-type-specific sensitivity, particle size effects, and the absence of capping agents in our synthesis, rather than intrinsic nanoparticle superiority. The effective biocompatibility of our microwave-synthesized AgNPs likely arises from three factors: (i) the absence of capping agents eliminates coating-dependent cytotoxicity; (ii) the 77.4 nm spherical morphology provides effective bacterial contact while limiting excessive mammalian cell penetration. Nonetheless, determining the absolute optimal particle size requires further research; and (iii) the rapid 30-minute bactericidal action minimizes cumulative exposure duration for host cells. This favorable therapeutic window, eradicating pathogenic bacteria at concentrations well below the half-maximal cytotoxic dose, positions these AgNPs as promising candidates for safe wound healing and as a supplementary ingredient for endodontic disinfection [37], safely eradicating pathogens while preserving osteoblasts.

4. Conclusion

The microwave-assisted AgNPs synthesized in this study demonstrate an exceptional therapeutic profile, combining rapid antibacterial efficacy against *E. coli* and *S. aureus* at 50 µg/ml within 30 minutes, and achieving ≥ 4-$\log_{10}$ reduction to below the assay detection limit (< 10 CFU/ml) with remarkable osteoblastic biocompatibility. Notably, the IC_{50} value remained above 50 µg/ml at 48 h for MC3T3-E1 cells. The retention of 75.5% MC3T3-E1 viability at the antibacterial working concentration (50 µg/ml) and 48 h demonstrate that effective bacterial elimination can be achieved without severe cytotoxicity in preosteoblasts. However, the observed time-dependent decrease in IC_{50} at 72 h (~48.3 µg/ml) highlights the importance of controlled exposure duration in therapeutic applications. This effective biocompatibility, which may be associated with the absence of capping agents, uniform spherical morphology (77.4 ± 12 nm), and rapid bactericidal action minimizing cellular exposure, establishes a wide therapeutic window that is particularly advantageous for wound healing and regenerative endodontics, particularly as a supplementary ingredient for disinfecting the root canal system, where eradicating bacteria while strictly preserving osteoblast viability is paramount.

Acknowledgment

The authors gratefully acknowledge the help of Mr. Amir Zali in performing the XRD measurements. The support received from the Iranian Research Organization for Science and Technology (IROST) under grant number 046039 is gratefully acknowledged.

References

1. S. Gujjar, S. Kukal, P. Jayabal, N. Balaji, S. Sainger, S. Roy, S. Rallapalli, R. Mahadevappa, S. Minocha, S. Kumar, S. Mathapati, Nanomaterials for biomedical applications: Addressing regulatory hurdles and strategic solutions, Nano Trends 11 (2025).
2. M. Abdullah, M. Obayedullah, M. Shariful Islam Shuvo, M. Abul Khair, D. Hossain, M. Nahidul Islam, A review on multifunctional applications of nanoparticles: Analyzing their multi-physical properties, Results in Surfaces and Interfaces 21 (2025).
3. G. Vijayakumar, E. Thangavel, D. Alshamsi, M. Sherif, A.A. Murad, S. Sangaraju, A critical review on the prospective role of nanomaterials in the effectual removal of radionuclides from wastewater – State of the art and future challenges, Environ. Technol. Innov. 38 (2025).
4. R.A. Alzahrani, F.G. Alhaddad, E.O. Alshammari, F.S. Alsowaileh, M.D. Alghamdi, A. Modwi, M.N. Goda, L.S. Alqarni, Silver nanoparticles in gas sensing: A comprehensive review of synthesis, mechanisms, performance metrics, and emerging applications, Journal of Science: Advanced Materials and Devices 10 (2025).
5. A. Dhaka, S. Chand Mali, S. Sharma, R. Trivedi, A review on biological synthesis of silver nanoparticles and their potential applications, Results Chem. 6 (2023).
6. R. Garg, P. Rani, R. Garg, M.A. Khan, N.A. Khan, A.H. Khan, J.H.P. Américo-Pinheiro, Biomedical and catalytic applications of agri-based biosynthesized silver nanoparticles, Environmental Pollution 310 (2022).
7. P. Pachghare, D. Zambre, D. Malode, M. Kale, N. Wankhede, R. Trivedi, M. Umekar, N. Raut, Combating multi-drug resistance with silver nanoparticles: A systematic review, Microbe (Netherlands) 9 (2025).
8. S. V. Khairnar, A. Das, D. Oupický, M. Sadykov, S. Romanova, Strategies to overcome antibiotic resistance: silver nanoparticles and vancomycin in pathogen eradication, RSC Pharmaceutics 2 (2025) 455–479.
9. S. Wahab, T. Khan, M. Adil, A. Khan, Mechanistic aspects of plant-based silver nanoparticles against multi-drug resistant bacteria, Heliyon 7 (2021).
10. M. Ozdal, S. Gurkok, Recent advances in nanoparticles as antibacterial agent, ADMET DMPK 10 (2022) 115–129.
11. S. Fallah, E. Yusefi-Tanha, J.R. Peralta-Videa, Interaction of nanoparticles and reactive oxygen species and their impact on macromolecules and plant production, Plant Nano Biology 10 (2024).
12. D. Das, P. Paul, Environmental impact of silver nanoparticles and its sustainable mitigation by novel approach of green chemistry, Plant Nano Biology 14 (2025).
13. A. Thakur, R. Ganesan, J. Ray Dutta, Nanomaterials against antimicrobial resistance and beyond: toward mitigating bacterial resuscitation, Total Environment Microbiology 2 (2026) 100052.
14. V.R. Manikam, K.Y. Cheong, K.A. Razak, Chemical reduction methods for synthesizing Ag and Al nanoparticles and their respective nanoalloys, Materials Science and Engineering: B 176 (2011) 187–203.
15. M. Fahim, A. Shahzaib, N. Nishat, A. Jahan, T.A. Bhat, A. Inam, Green synthesis of silver nanoparticles: A comprehensive review of methods, influencing factors, and applications, JCIS Open 16 (2024).
16. N.A. Singh, J. Narang, D. Garg, V. Jain, D. Payasi, S. Suleman, R.K. Swami, Nanoparticles synthesis via microorganisms and their prospective applications in agriculture, Plant Nano Biology 5 (2023).
17. A. Umar, R.H.R. Syam, W. Handayani, N. Qaiser, D.O.B. Apriandanu, Y. Yulizar, Modification of silver nanoparticles (AgNPs) with tollens reagent for selective colorimetric detection of formaldehyde, Results Chem. 17 (2025).
18. R. Moradi, H. Ahmadi, M.R. Barati, S.F. Kashani-Bozorg, Development of Ag/Mg(1-x)ZnxFe2O4nanocomposites via microwave-assisted synthesis: Combining biocompatibility with superior bacterial inactivation for water disinfection, J. Environ. Chem. Eng. 13 (2025).
19. M.R. Barati, Influence of zinc substitution on magnetic and electrical properties of MgCuZn ferrite nanocrystalline powders prepared by sol-gel, auto-combustion method, J. Alloys Compd. 478 (2009) 375–380.
20. V.S. Ramkumar, A. Pugazhendhi, K. Gopalakrishnan, P. Sivagurunathan, G.D. Saratale, T.N.B. Dung, E. Kannapiran, Biofabrication and characterization of silver nanoparticles using aqueous extract of seaweed Enteromorpha compressa and its biomedical properties, Biotechnology Reports 14 (2017) 1–7.
21. S.S. Rao, K. Saptami, J. Venkatesan, P.D. Rekha, Microwave-assisted rapid synthesis of silver nanoparticles using fucoidan: Characterization with assessment of biocompatibility and antimicrobial activity, Int. J. Biol. Macromol. 163 (2020) 745–755.
22. M. Oves, M. Aslam, M.A. Rauf, S. Qayyum, H.A. Qari, M.S. Khan, M.Z. Alam, S. Tabrez, A. Pugazhendhi, I.M.I. Ismail, Antimicrobial and anticancer activities of silver nanoparticles synthesized from the root hair extract of Phoenix dactylifera, Materials Science and Engineering C 89 (2018) 429–443.
23. B. Ajitha, Y. Ashok, K. Reddy, K.M. Rajesh, P. Sreedhara Reddy, Sesbania grandiflora leaf extract assisted green synthesis of silver nanoparticles: Antimicrobial activity, 2016.
24. O.T. Jemilugba, E.H.M. Sakho, S. Parani, V. Mavumengwana, O.S. Oluwafemi, Green synthesis of silver nanoparticles using

Combretum erythrophyllum leaves and its antibacterial activities, Colloids and Interface Science Communications 31 (2019).
25. C. Iwuji, H. Saha, W. Ghann, D. Dotson, M.A.K. Bhuiya, M.S. Parvez, Z.S. Jahangir, M.M. Rahman, F.I. Chowdhury, J. Uddin, Synthesis and characterization of silver nanoparticles and their promising antimicrobial effects, Chemical Physics Impact 9 (2024).
26. S. Bhattacharjee, G. Debnath, A.R. Das, A.K. Saha, P. Das, Characterization of silver nanoparticles synthesized using an endophytic fungus, Penicillium oxalicum having potential antimicrobial activity, Advances in Natural Sciences: Nanoscience and Nanotechnology 8 (2017).
27. A. Lateef, B.I. Folarin, S.M. Oladejo, P.O. Akinola, L.S. Beukes, E.B. Gueguim-Kana, Characterization, antimicrobial, antioxidant, and anticoagulant activities of silver nanoparticles synthesized from Petiveria alliacea L. leaf extract, Prep. Biochem. Biotechnol. 48 (2018) 646–652.
28. R. Pérez-Tanoira, M. Fernández-Arias, C. Potel, R. Carballo-Fernández, S. Pérez-Castro, M. Boutinguiza, M. Górgolas, F. Lusquiños, J. Pou, Silver Nanoparticles Produced by Laser Ablation and Re-Irradiation Are Effective Preventing Peri-Implantitis Multispecies Biofilm Formation, Int. J. Mol. Sci. 23 (2022).
29. S.M. Lee, K.C. Song, B.S. Lee, Antibacterial activity of silver nanoparticles prepared by a chemical reduction method, Korean Journal of Chemical Engineering 27 (2010) 688–692.
30. T. Kathiraven, A. Sundaramanickam, N. Shanmugam, T. Balasubramanian, Green synthesis of silver nanoparticles using marine algae Caulerpa racemosa and their antibacterial activity against some human pathogens, Applied Nanoscience (Switzerland) 5 (2015) 499–504.
31. E. Urnukhsaikhan, B.E. Bold, A. Gunbileg, N. Sukhbaatar, T. Mishig-Ochir, Antibacterial activity and characteristics of silver nanoparticles biosynthesized from Carduus crispus, Sci. Rep. 11 (2021).
32. S.P.R.D.R.J.M. and S.K. Rajesh, Biosynthesis ofsilver nanoparticles using Ulva fasciata(Delile) ethyl acetate extract and its activity against Xanthomonas campestris pv. malvacearum., Journal of Biopesticide 5(0) (2012) 119–128.
33. M.A. Haque, R. Imamura, G.A. Brown, V.R. Krishnamurthi, I.I. Niyonshuti, T. Marcelle, L.E. Mathurin, J. Chen, Y. Wang, An experiment-based model quantifying antimicrobial activity of silver nanoparticles on: Escherichia coli, RSC Adv. 7 (2017) 56173–56182.
34. Y.Y. Loo, Y. Rukayadi, M.A.R. Nor-Khaizura, C.H. Kuan, B.W. Chieng, M. Nishibuchi, S. Radu, In Vitro antimicrobial activity of green synthesized silver nanoparticles against selected Gram-negative foodborne pathogens, Front. Microbiol. 9 (2018).
35. B. Dinç, Comprehensive toxicity assessment of silver nanoparticles on Bacteria, human vein endothelial cells, and Caenorhabditis Elegans, Results in Chemistry 14 (2025) 102092.
36. M. Paknejadi, M. Bayat, M. Salimi, V. Razavilar, Concentration- and Time-Dependent Cytotoxicity of Silver Nanoparticles on Normal Human Skin Fibroblast Cell Line, Iranian Red Crescent Medical Journal (IRCMJ) (2018) 1–8.
37. F. Afhkami, P. Ahmadi, G. Rostami, Cytotoxicity of Different Concentrations of Silver Nanoparticles and Calcium Hydroxide for MC3T3-E1 Preosteoblast Cell Line, Clinical and Experimental Dental Research 11(1) (2025) e70075.